HIGH-FREQUENCY VOLTAGE-CONTROLLED CONTINUOUS-TIME LOWPASS FILTER USING LINEARISED CMOS INTEGRATORS

Indexing term: Filters

The design and implementation of a continuous-time lowpass filter with voltage-controlled cutoff frequency and passband ripple is presented. The circuit uses a linearised CMOS transconductor as a basic integrating building block. A voltage-controlled phase-adjusting scheme is employed in the integrator to compensate for excess phase in the transconductance at high frequencies. The fabricated filter is capable of realising cutoff frequencies as high as 2 MHz and handles single-ended input signals up to 4 V p–p with less than 1% distortion.

Introduction: Recently several techniques for realising continuous-time filters in MOS technology have been proposed. Most of these techniques realise filters in the audio frequency range,[1] where switched-capacitor (SC) circuits have already been established as a viable approach. However, as operating frequencies are raised by an order of magnitude or more, the advantages of continuous-time processing become increasingly apparent.[2] To date, only a few fully MOS realisations of high-frequency continuous-time filters have been reported. The technique proposed in Reference 2 realises a 500 kHz bandpass filter but has limited signal swing capability due to nonlinearities in the MOSFETs used. Recently, a low-frequency linearising scheme has been extended to high frequencies,[3] but only simulated results using operational amplifiers with 200 MHz gain-bandwidth products are available. This letter discusses the implementation of a 1 MHz lowpass filter using linearised CMOS transconductance integrators with improved signal-handling capability. Experimental results obtained from a fabricated test chip are reported.

Filter realisation: Fig. 1 shows the basic transconductance circuit used in the proposed filter. It employs a linearised input stage consisting of a simple source-coupled pair M_1, M_2 biased dynamically by a current component proportional to the square of the input voltage $V = V_1 - V_2$. This square-law current is generated by the crosscoupled configuration M_3–M_6 and coupled through a level-shifting device M_7. By properly scaling the W/L ratios of the source-coupled pair and the crosscoupled devices, the nonlinearities of the input stage can be largely cancelled out over a wide input voltage range.[4] The remaining devices M_8–M_{31} are used to bias the input stage and to sum device currents to obtain the final output current I_o. Assuming unity-gain current mirrors and a square-law model[5] for the input devices gives the following linear i/v characteristic for the complete transconductor:

$$I_o = g_m V = K(V_C - V_{Tn})V \tag{1}$$

where K is a constant dependent on process parameters and the geometries of M_1–M_6 and M_8–M_{11}, and V_{Tn} is the n-channel threshold voltage. Note that the transconductance $g_m = K(V_C - V_{Tn})$ is adjustable by control voltage V_C. The range of V over which eqn. 1 is valid and further design details for the basic input stage are discussed elsewhere[4] and are not repeated here.

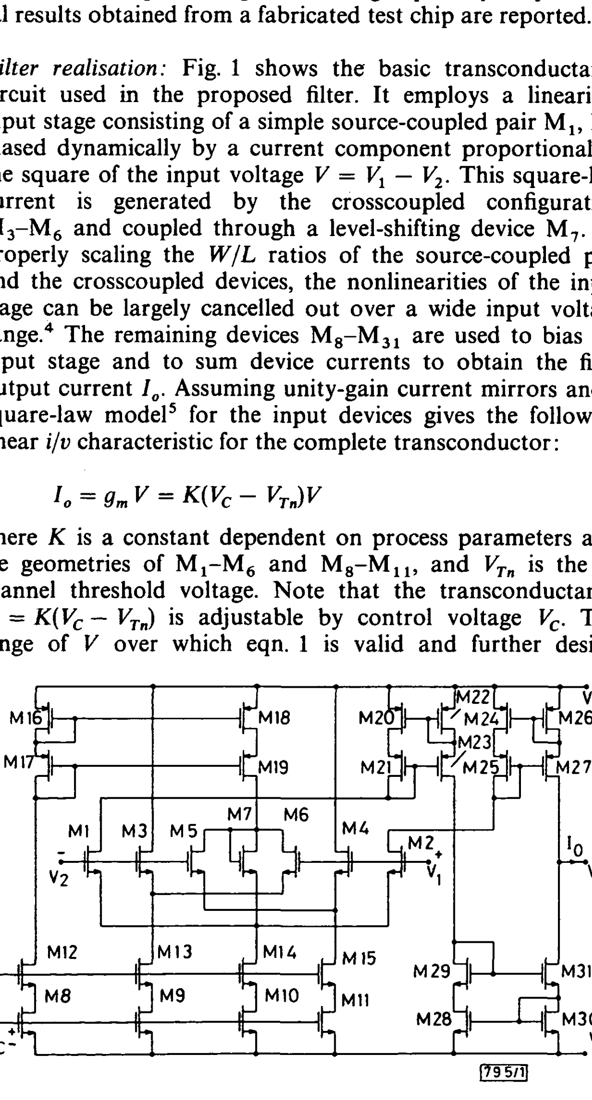

Fig. 1 *Linearised CMOS transconductance circuit*

The complete transconductance circuit of Fig. 1 was fabricated using a standard 3 μm double-poly p-well CMOS process.[6] M_1, M_2 and M_5–M_7 had $W/L = 10\ \mu m/5\ \mu m$ while M_3, M_4 had $W/L = 20\ \mu m/5\ \mu m$. The substrates of these devices were connected to their respective sources. The remaining n-channel devices were in a common p-well connected to V_{SS}. All p-channel devices shared a common substrate connected to V_{DD}. The circuit occupies a total area of $220 \times 700\ \mu m^2$. Fig. 2 depicts the nonlinearity in the measured i/v characteristics of the fabricated circuit as a percentage of a 2 V (peak) full-scale value, using the nominal supply and bias voltage values indicated. The results are comparable to those for recently reported transconductor schemes.[7,8]

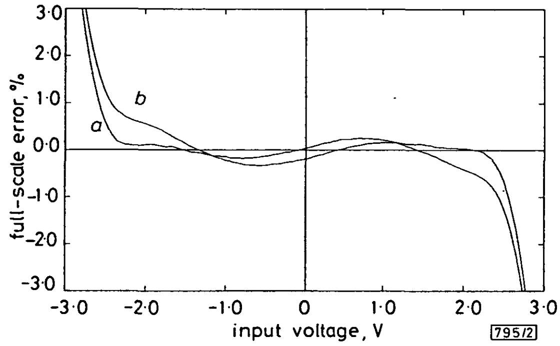

Fig. 2 *Measured nonlinear error of transconductor for $V_{DD} = -V_{SS} = 5$ V, $V_B = -2{\cdot}5$ V, $V_C = 1{\cdot}75$ V, $V_o = 0$*

a Input V_1, $V_2 = 0$
b Input V_2, $V_1 = 0$

However, the present circuit has the advantage of not requiring an accurately balanced input drive or a complicated output common-mode biasing circuit.[2] The circuit consumes 10 mW with the nominal bias values, and exhibits a short-circuit 3 dB bandwidth of 15 MHz.

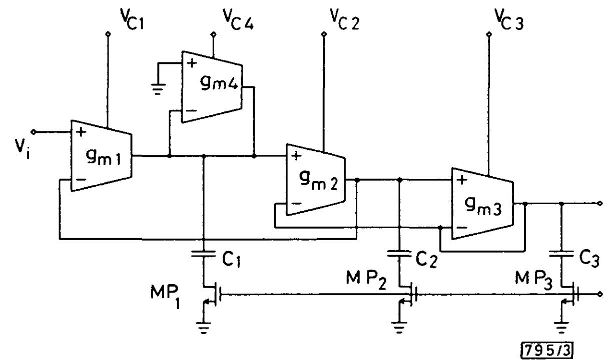

Fig. 3 *3rd-order Chebyshev lowpass filter using phase-compensated transconductance integrators*

$g_{m1} = g_{m2} = g_{m3} = g_{m4} = g_m$, $C_1 = C_3 \simeq 9{\cdot}2$ pF, $C_2 \simeq 4{\cdot}5$ pF

Fig. 3 shows a 3rd-order Chebyshev lowpass ladder filter realised using the transconductor of Fig. 1 as a basic integrating building block. MOS capacitors C_1–C_3 perform the required integration. The drain resistances of devices MP_1–MP_3 in series with the capacitors introduce a high-frequency zero in the transfer function of each integrator. This zero is used to compensate for excess phase shift within the transconductor at high frequencies. The location of this zero is controllable using V_P, resulting in a voltage-variable phase-compensation scheme. If the initial phase errors are not large, the zero frequency is much higher than the unity-gain bandwidth of the integrator. Therefore, at frequencies within the passband of the filter, the signal voltages across the compensating MOSFETs are very small, resulting in negligible distortion due to nonlinearities of these devices. It can be shown that, for a single integrator with input $V = V_A \sin \omega t$, the distortion caused by the nonlinear phase-compensating device is mainly due to the second-harmonic component and is approximately given by

$$HD \simeq \frac{(g_m r_d)^2 V_A}{(V_P - V_{Tn})\sqrt{4(g_m r_d)^2 + (g_m/\omega C)^2}} \tag{2}$$

where g_m is the integrator transconductance, C the integrating capacitance and r_d the small-signal resistance of the compensating transistor. Eqn. 2 has been derived assuming a first-order model of the compensating MOSFET operating in the ohmic region of its i/v characteristic.[5] For typical values $g_m r_d = 0{\cdot}02$, $V_A = V_P - V_{Tn} = 2$ V and $\omega = g_m/C$, eqn. 2 gives $HD < 0{\cdot}05\%$.

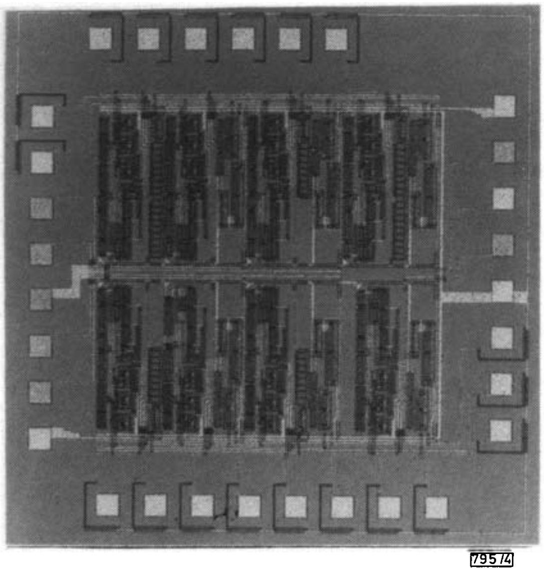

Fig. 4 *Photomicrograph of experimental chip*

The complete filter of Fig. 3 was designed to have a nominal cutoff frequency $f_c = 1$ MHz with a passband ripple of 1 dB and was fabricated using the process already mentioned.[6] MP_1–MP_3 had $W/L = 25$ and their substrates were short-circuited to their sources. The entire filter, including the capacitances, phase-compensating devices and on-chip output buffers, occupies an area of 1500 × 700 μm^2. A photomicrograph of an experimental chip including the proposed filter as well as single transconductor and buffer test cells is shown in Fig. 4. All measurements were made using ± 5 V supplies with $V_B = -2{\cdot}5$ V. Fig. 5*a* shows the measured frequency response of the 1 MHz filter after adjusting $V_{C1} = V_{C2} = V_{C3} = V_{C4} = V_C$ and V_P to obtain the specified cutoff frequency and passband ripple. Expanded passband characteristics are given in Fig. 4*b* for four different values of (V_C, V_P) corresponding to f_c ranging from 250 kHz to 2 MHz. In each case the control voltages were adjusted to make the measured passband response within 0·1 dB of the ideal Chebyshev response. For f_c as high as 1·5 MHz, the variation in cutoff frequency is essentially linear with respect to V_C, as expected from the linear dependence of g_m in eqn. 1. Above this frequency, the increased value of V_C required drives M_8–M_{11} into their ohmic regions of operation, resulting in a nonlinear dependence of f_c on V_C. This also limits the maximum obtainable value of f_c to approximately 2·2 MHz. To test the effectiveness of the phase control scheme, the drain resistances of MP_1–MP_3 were made very small by applying a large V_P (+10 V). This effectively disabled the phase compensation and resulted in a 2 dB peaking at the edge of the passband due to excess phase shifts in the integrators. The distortion characteristics of the filter were investigated. Fig. 6 shows the output spectrum obtained for the 1 MHz filter with a 4 V p–p input signal at 250 kHz. The total harmonic distortion in this case is within 1%. This distortion is reduced to 0·2% for a 2 V p–p input. The measured output noise spectral density above 10 kHz in the passband of the 1 MHz filter is fairly constant at 0·1 $\mu V/\sqrt{(Hz)}$. This value increases slightly at lower frequencies due to $1/f$ noise, rising to 1 $\mu V/\sqrt{(Hz)}$ at 100 Hz.

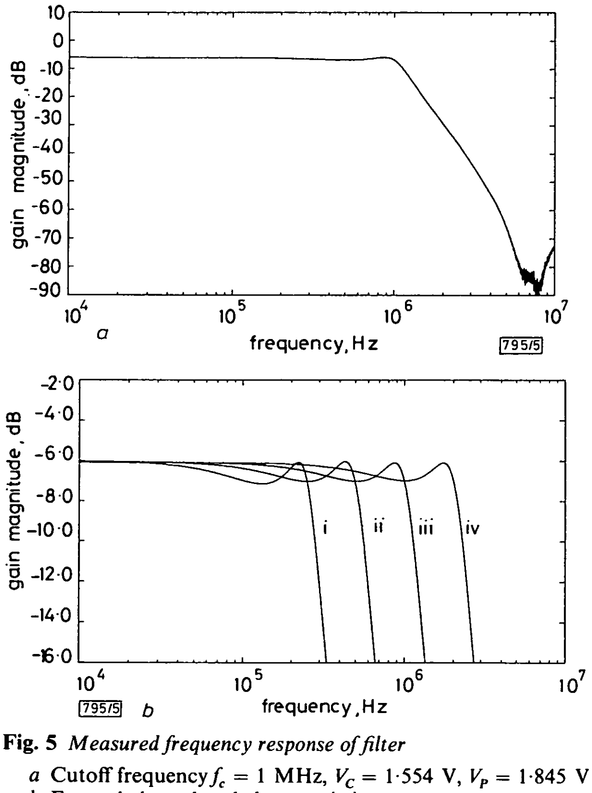

Fig. 5 *Measured frequency response of filter*

a Cutoff frequency $f_c = 1$ MHz, $V_C = 1{\cdot}554$ V, $V_P = 1{\cdot}845$ V
b Expanded passband characteristics:
(i) $f_c = 250$ kHz, $V_C = 1{\cdot}155$ V, $V_P = 1{\cdot}065$ V
(ii) $f_c = 500$ kHz, $V_C = 1{\cdot}288$ V, $V_P = 1{\cdot}270$ V
(iii) $f_c = 1$ MHz, $V_C = 1{\cdot}554$ V, $V_P = 1{\cdot}845$ V
(iv) $f_c = 2$ MHz, $V_C = 2{\cdot}562$ V, $V_P = 4{\cdot}320$ V

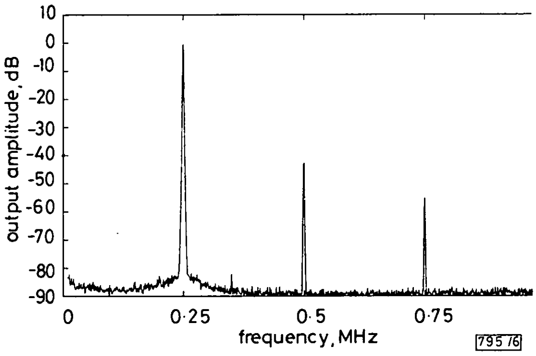

Fig. 6 *1 MHz filter output distortion spectrum for $V_i = 4$ V p–p at 250 kHz*

Conclusion: The design and implementation of a novel continuous-time filter technique using linearised high-frequency CMOS transconductors has been presented. A fabricated Chebyshev lowpass prototype exhibits a 1 MHz nominal cutoff frequency and is capable of handling input signals as high as 4 V p–p with less than 1% distortion using ± 5 V supplies. Using a voltage-controlled phase-compensation scheme, accurate response can be obtained for cutoff frequencies as high as 2 MHz. The voltage-control feature allows the filter to be tuned on-chip against process and temperature variations using known tuning schemes. Extension of this technique to higher frequencies is currently being investigated.

A. P. NEDUNGADI
R. L. GEIGER

Department of Electrical Engineering
Texas A&M University
College Station, TX 77843, USA

12th May 1986

References

1 TSIVIDIS, Y., BANU, M., and KHOURY, J.: 'Continuous-time MOSFET-C filters in VLSI', *IEEE Trans.*, 1986, **CAS-33**, pp. 125–140
2 KHORRAMABADI, H., and GRAY, P. R.: 'High-frequency CMOS continuous-time filters', *IEEE J. Solid-State Circuits*, 1984, **SC-19**, pp. 939–948
3 KHOURY, J., SHI, B-X, and TSIVIDIS, Y.: 'Considerations in the design of high frequency fully integrated continuous time filters'. IEEE international symposium on circuits and systems, 1985
4 NEDUNGADI, A., and VISWANATHAN, T. R.: 'Design of linear CMOS transconductance elements', *IEEE Trans.*, 1984, **CAS-31**, pp. 891–894
5 PENNEY, W. M., and LAU, L.: 'MOS integrated circuits' (Van Nostrand Reinhold, New York, 1972), pp. 60–70

6 'MOSIS User's Manual'. USC Information Sciences Inst., Marina Del Rey, CA, 1985

7 FERNANDEZ, F. J., and SCHAUMANN, R.: 'Techniques for the design of linear CMOS transconductance elements for video-frequency applications'. Midwest symposium on circuits and systems, 1985

8 TSIVIDIS, Y., CZARNUL, Z., and FANG, S. C.: 'MOS transconductors and integrators with high linearity', *Electron. Lett.*, 1986, **22**, pp. 245–246

COMMENT

WIDEBAND FREQUENCY RESPONSE MEASUREMENT OF PHOTODETECTORS USING OPTICAL HETERODYNE DETECTION TECHNIQUE

Kawanishi and Saruwatari[A] report some interesting results about the measurement of photodiode bandwidths using the heterodyne technique.

I do not think, however, that their statement, 'A novel wideband frequency-response measurement system ...' is absolutely correct. In fact, I believe that their method is similar to that reported in Reference B, the only differences being the operating wavelength (850 nm instead of 1·3 μm), the use of conventional single-mode Fabry–Perot laser diodes instead of DFB lasers, and the mixing of the two beams obtained by means of a beam splitter rather than by a fibre coupler.

P. SPANO

Fondazione 'Ugo Bordoni'
Viale di Trastevere, 108
00153 Roma, Italy

24th April 1986

REPLY

We are grateful for Dr. Spano's comment. It is true that our experiment was based on the optical heterodyne detection technique. The first experiment with GaAs/AlGaAs semiconductor lasers was made by Dr. L. Picarri and Dr. P. Spano.

In our letter it has been shown that the polarisation-maintaining single-mode fibre coupler and the isolator stabilised the shape of the beat signal and the DFB-LDs made it possible to continuously sweep the beat frequency up to some tens of gigahertz without longitudinal mode-hopping, resulting in wideband precise measurement of the frequency response of photodetectors.

S. KAWANISHI
M. SARUWATARI

NTT Electrical Communications Laboratories
1-2356. Take
Yokosuka-shi, Kanagawa-ken 238-03, Japan

30th May 1986

References

A KAWANISHI, S., and SARUWATARI, M.: 'Wideband frequency response measurement of photodetectors using optical heterodyne detection technique', *Electron. Lett.*, 1986, **22**, (6), pp. 337–338

B PICCARI, L., and SPANO, P.: 'New method for measuring ultrawide frequency response of optical detectors', *ibid.*, 1982, **18**, pp. 116–118

HIGH RETURN LOSS CONNECTOR DESIGN WITHOUT USING FIBRE CONTACT OR INDEX MATCHING

Indexing terms: Optical fibres, Optical connectors and couplers

A noncontacting connector design which reduces the returned power from reflections is demonstrated. The design takes advantage of the poor coupling characteristics between tilted Gaussian beam modes of single-mode fibre. The connector's mean return loss is −38 dB and its mean insertion loss is 0·7 dB.

Introduction: Optical feedback can degrade laser signal quality by inducing intensity fluctuations[1] and frequency shifts.[2] These effects will become increasingly penalising as fibre system bit rates increase.[3] Since connector reflections are a major source of optical feedback in a system, the suppression of these reflections is particularly important for high bit rate systems. In contacting connectors, reflections are reduced by bringing the fibre faces into intimate contact. The reflections in this case are usually in the vicinity of −30 dB and are limited by the integrity of contact practically achievable.[4] In this letter we present a design with which mean reflections of −38 dB are demonstrated without bringing the fibres into contact. This design has been incorporated into the biconic connector and designated as the SPA biconic connector.

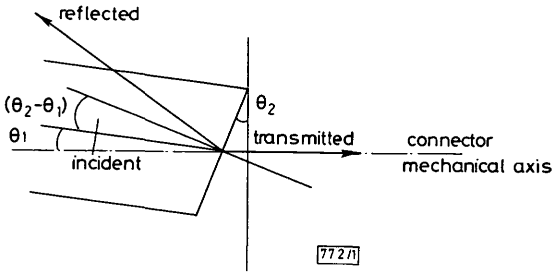

Fig. 1 *Schematic representation of operating principle*

Principle of operation: The operating principle of the design is illustrated in Fig. 1. The fibre is tilted at an angle θ_1 with respect to the mechanical axis of the connector. The face of the connector is polished at an angle θ_2 to the axis normal to refract the light emanating from the fibre end on to the mechanical axis of the connector. Snell's law applied at the face of the fibre yields the following expression relating the tilt and polish angles:

$$\tan\theta_2 = \frac{\sin\theta_1}{\cos\theta_1 - \dfrac{1}{n}} \tag{1}$$

where n is the refractive index of the fibre. The reflected beam at the fibre/air interface is reflected at an angle of $2(\theta_2 - \theta_1)$ to the axis of the fibre, causing poor coupling into the guided mode of the fibre. The mode of a single-mode fibre has been shown to be very nearly Gaussian in shape.[5] The coupling efficiency of the reflected beam into the guided mode can, therefore, be calculated using Gaussian mode-matching equations. For a fibre of spot size ω, the coupling efficiency C of a beam reflected at an angle ϕ to the axis of the fibre can be shown to be given by[5]

$$C = \exp -\left(\frac{\pi n \omega \phi}{\lambda}\right)^2 \tag{2}$$

where λ is the wavelength.

Fabrication and results: SPA biconical connectors were fabricated by moulding the fibre hole at an angle θ_1 to the axis of biconical connector plugs and polishing the fibre face at an angle θ_2 to the connector axis normal. Return loss measure-

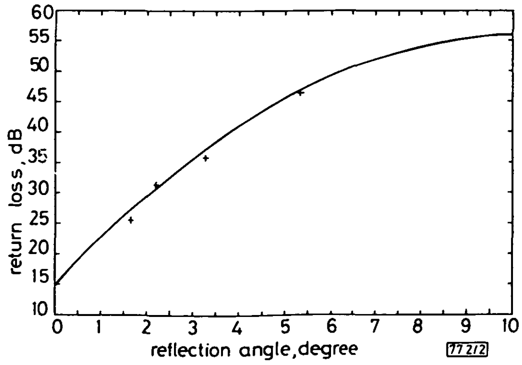

Fig. 2 *Experimental values and theoretical plot of return loss against reflection angle*